ACS APPLIED MATERIALS & INTERFACES

RESEARCH ARTICLE

www.acsami.org

Adsorption and Association of a Symmetric PEO-PPO-PEO Triblock Copolymer on Polypropylene, Polyethylene, and Cellulose Surfaces

Yan Li,[†,▽] Hongyi Liu,[∥] Junlong Song,[‡] Orlando J. Rojas,[§,⊥] and Juan P. Hinestroza*[,†]

[†]Department of Fiber Science and Apparel Design, Cornell University, Ithaca, New York 14853, United States

[∥]Department of Earth and Atmospheric Science, Cornell University, Ithaca, New York 14853, United States

[‡]Jiangsu Provincial Key Lab of Pulp and Paper Science and Technology, Nanjing Forestry University, Nanjing, Jiangsu, 210037, P.R.China

[§]Department of Forest Biomaterials, North Carolina State University, Campus Box 8005, Raleigh, North Carolina 27695-8005, United States

[⊥]Department of Forest Products Technology, Faculty of Chemistry and Materials Sciences, Helsinki University of Technology, P.O. Box 3320, FIN-02015 TKK, Espoo, Finland

ABSTRACT: The association of a symmetric polyoxyethylene-polyoxypropylene-polyoxyethylene (PEO_{19}—PPO_{29}—PEO_{19}) triblock copolymer adsorbed from aqueous solutions onto polypropylene (PP), polyethylene (PE), and cellulose surfaces was probed using Atomic Force Microscopy (AFM). Significant morphological differences between the polyolefin substrates (PP and PE) and the cellulose surfaces were observed after immersion of the films in the PEO_{19}—PPO_{29}—PEO_{19} solutions. When the samples were scanned, while immersed in solutions of the triblock copolymer, it was revealed that the structures adsorbed on the polyolefin surfaces were smoothed by the adsorbed PEO_{19}—PPO_{29}—PEO_{19}. In contrast, those structures on the hydrophilic cellulose surfaces were sharpened. These observations were related to the roughness of the substrate and the energy of interaction between the surfaces and the PEO and PPO polymer segments. The interaction energy between each of the blocks and the surface was calculated using molecular dynamics simulations. It is speculated that the associative structures amply reported in aqueous solution at concentrations above the critical micelle concentration, CMC, are not necessarily preserved upon adsorption; instead, it appears that molecular arrangements of the anchor-buoy type and hemimicelles prevail. The reported data suggests that the roughness of the surface, as well as its degree of hydrophobicity, have a large influence on the nature of the resulting adsorbed layer. The reported observations are valuable in explaining the behavior of finishing additives and lubricants commonly used in textile and fiber processing, as well as the effect of the morphology of the boundary layers on friction and wear, especially in the case of symmetric triblock copolymers, which are commonly used as antifriction, antiwear additives.

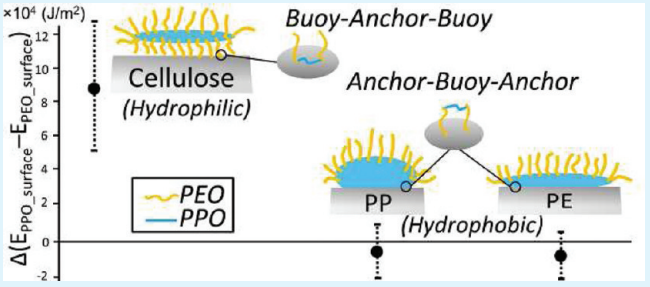

KEYWORDS: adsorption, self-assembly, triblock copolymer, atomic force microscopy, hemimicelles, textile finishing, liquid imaging

1. INTRODUCTION

The morphology and chemical interactions between finishes and fiber surfaces are critical in understanding boundary lubrication phenomena in textile and fiber processing. In typical applications, self-assembled thin layers are formed at the interface between the solution and the surface. These adsorbed boundary layers have been shown to control surfaces properties such as surface energy, wettability, as well as friction and wear resistance.[1]

Current understanding of boundary lubrication in textiles processing is very limited and mainly based on empirical observations. In fact, only a few reports are available addressing adsorption of finishes and its associated nanoscale phenomena in textile fibers. The early attempts to study lubrication on textile fibers appear to have been led by Perwelz and co-workers who related changes in the friction coefficient of polypropylene (PP) filaments to alternating stick—slip cycles.[2,3] Perwelz et al. suggested that lubricant molecules might self-assemble on the surface by aligning themselves in distinctive ways, depending on the nature of the involved chemical and physical interactions. It was noted that hydroxylated oils with rigid backbone structures induced higher friction forces than flexible molecules. In particular, the friction coefficients measured on a fiber lubricated with hydroxylated oleate ($CH_3(CH_2)_7CH{=}CH(CH_2)_7COOH$) were higher than those for a fiber coated with hydroxylated stearate ($CH_3(CH_2)_{16}COOH$).[2] The difference in lubrication performance was attributed to molecular features, such as backbone rotation and flexibility brought by the saturated hydrocarbon in the stearate molecules. However, no direct

Received: March 2, 2011
Accepted: May 19, 2011
Published: May 19, 2011

evidence has been presented to validate these speculations. The reported efforts were clearly aimed at linking macroscopic friction behavior with the molecular structure of the respective lubricant.[3]

The surface force apparatus (SFA) has been widely used in tribology studies.[4] SFA is based on optical interferometry enabling the measurement of surface forces on mica, silica, and alumina, among others.[4−6] However, the application of SFA and other techniques to study polymeric materials such as those relevant to textile and fiber processing is limited and thus a fundamental understanding of fiber tribology at the nanoscale is lacking. Recently, the atomic force microscopy (AFM) has been used to probe lubrication phenomena at resolutions that are higher than that of conventional techniques familiar to the fiber and finishes industries.[7] There is a significant number of reported AFM-based tribology studies aimed at probing friction behavior on hard surfaces such as mica,[4] silica,[8] and graphite.[9] Furthermore, these and other studies have shown distinctive correlations between lubrication performance and properties such as molecular weight,[10] chemical composition,[11] and viscoelasticity of the adsorbed lubricant.[12]

Lubricants commonly used in textile processing are usually composed of fatty acids, mineral oils, and synthetic compounds, such as ethoxylated alcohols, ethoexylated acids, and silicone fluids.[2] Surface active triblock hydrocarbon polymers consisting of polyoxyethylene (PEO) and polyoxypropylene (PPO) are also commonly used in formulations of fiber lubricants. These copolymers are of interests as they adsorb on hydrophobic surfaces with the more hydrophobic PPO acting as an anchor chain while the hydrophilic PEO units extending into solution as tails.[13] Li et al. used photon correlation spectroscopy and electron spin resonance techniques to conclude that upon adsorption of Pluronic polymers the PEO tails were in a relaxed state between a fully extended chain and a random coil conformation.[14] By using surface forces and optical measurements Schillen et al. found a similar head−tail configuration for diblock copolymers of polyoxyethylene−polyoxybutylene adsorbed on hydrophobized mica.[15]

THEORETICAL MODELS OF SELF-ASSEMBLIES ON POLYMER SURFACES

Triblock copolymers of PEO−PPO−PEO are commonly used in the formulation of detergents, emulsifiers, dispersants, stabilizers and lubricants as their physicochemical properties can be tailored by varying the ratio between the hydrophilic PEO and the hydrophobic PPO blocks.[16] Adsorption and desorption behaviors of triblock copolymers from aqueous solutions onto hard surfaces have been studied via ellipsometry,[17] total internal fluorescence spectroscopy (TIRF),[18] surface plasmon resonance spectroscopy (SPR),[19] and quartz crystal microgravimetry (QCM).[20]

Many investigators use a so-called buoy−anchor−buoy (B−A−B) model to describe the adsorption of triblock copolymers on hydrophobic surfaces.[14,21,22] In this B−A−B model, the hydrophobic PPO blocks are expected to strongly bind to the substrate, whereas the hydrophilic PEO blocks dangle in the aqueous solution from the surface forming a free "brush" layer. This B−A−B representation is derived from an earlier wetting model, which was used to describe adsorption of copolymers on hydrophobic surfaces.[23] Theoretical work, initially by Whitmore and later by Strove, studied several aspects of the adsorption and desorption of symmetric triblock copolymers including kinetics, thermodynamics, molecular configuration and micellization phenomena by using a scaling parameter σ^*as defined by eq 1.[19,21]

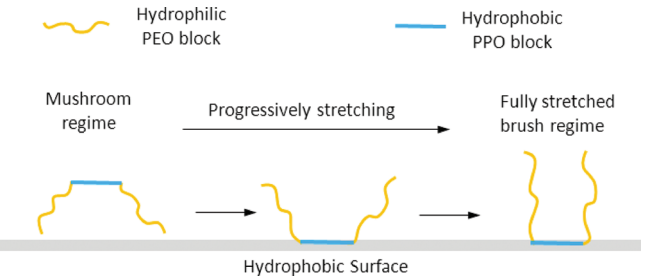

Figure 1. Schematic illustration of the buoy−anchor−buoy model for self-assembled structures formed by triblock copolymers on a hydrophobic surface. Three regimes are present, depending on the conformation of the hydrophilic PEO blocks: "mushroom", "progressively stretching", and "fully stretched" brush regimes. The transition between the three regimes is induced by increasing concentration of the triblock copolymer.[19,21−23].

$$\sigma^* = \frac{2\pi R_g^2}{\sum_{\text{area}}} \qquad (1)$$

σ^* is used to describe the surface density of the triblock copolymer covering a hydrophobic surface. In eq 1, R_g corresponds to the radius of gyration of a brush chain in solution, and Σ_{area} is the average number of molecules of the triblock copolymer present per unit area. σ^* is thus the ratio of the cross-sectional area of a free coiled chain in solution to the average area of a grafted chain.

Theoretical analysis indicates the existence of three main assembly regimes that depend on σ^*, as illustrated in Figure 1. One extreme case is the "mushroom" regime, which occurs when $\sigma^* \leq 2$. The σ^* value of the mushroom regime indicates a large average distance between polymer molecules. In the mushroom regime, the radius of gyration of the triblock copolymer determines the thickness of the layer of the molecular self-assemblies. The opposite case is the "brush" regime where $\sigma^* \geq 20$. In the brush regime, all dangling hydrophilic blocks stretch away from the hydrophobic surface into the solution. In this regime the average distance between anchoring polymer heads is much smaller than the lateral dimension of a single isolated polymer chain. The extended brush configuration shows characteristically high coverage density and large adsorption on the surface. A "progressively stretching" transition regime is expected if the value of σ^* falls in the range between 2 and 20, where the "mushroom" tails progressively unfolds to become highly stretched "brushes".

A very limited amount of reports addressing the adsorption of finishes, lubricants and additives, and the associated nanoscale phenomena, on materials commonly converted into fibers is currently available in the scientific literature. Most of the existing literature in the field is dedicated to adsorption phenomena in nondeformable rigid substrates. In particular, the adsorption of finishing or lubricant compounds onto PE and PP surfaces has not been previously studied at the nanoscale using atomic force microscopy neither the molecular interactions of these compounds with fiber-forming polymers have been elucidated. In this report, we aim at understanding the molecular configurations of adsorbed copolymers and their effect on the morphology of

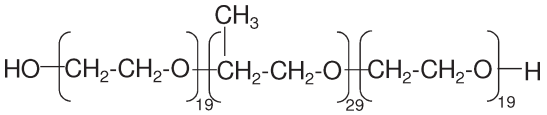

Figure 2. Chemical structure of triblock copolymer $EO_{19}PO_{29}EO_{19}$.

the adsorbed layers on substrates relevant to textile and fiber forming materials. In particular we used a triblock polymer of the Pluronic-type ($EO_{19}PO_{29}EO_{19}$) and ultrathin films of PP, PE, and cellulose as model surfaces.

The surface morphology of adsorbed triblock copolymers layers of was probed using atomic force microscopy (AFM) with imaging performed in air as well as in liquid medium (while the surfaces were immersed in the respective aqueous solution). Molecular dynamic (MD) simulations were used to predict the interaction energies and to quantitatively evaluate the affinity between the PEO−PPO−PEO triblock copolymers and the surfaces. Results from the MD results were used to gain insightful information about the self-assembled molecular structures that were observed under the AFM.

EXPERIMENTAL SECTION

Preparation of PP, PE, and Cellulose-Coated Surfaces. Three polymers (PP, PE, and cellulose) commonly spun into textile fibers were used in this study. PP and PE chips, obtained from Sigma Aldrich (St. Louis, MO) were dissolved in xylene (Sigma-Aldrich). The solution was heated and stirred for 2 h using a condensation system to reflux the evaporated solvent. Silica wafers (Waferworld, FL) were washed in Piranha solution and cleaned using an ultraviolet-ozone (UVO) treatment. An IR lamp was used to heat the surfaces of the silica wafers and the solution-delivery pipettes to a temperature of approximately 85 °C. The polymer solutions were spin-coated (WS-400A-6NPP, Laurell Technologies) onto the silica wafers at 2000 rpm for 20 s. The obtained samples were placed in an oven at 80 °C to evaporate residual solvent. XPS scans of the substrates were used to assess the chemical composition of the polymer films and to verify that no residual solvent was present.

Cellulose films were prepared employing the method reported by Song et al.[24] In this method polyvinylamide was used as an anchoring polymer to bind cellulose to the silica wafers. Clean silica wafers were immersed in a polyvinylamide (BASF Corp.) aqueous solution (100 ppm) for 20 min. The PVAm-coated surface was washed with Milli-Q water to remove excess PVAm and the surface was dried with nitrogen. 50 mg of Avicel microcrystalline cellulose was added to 2.5 mL of a N-methylmorpholine-N-oxide (NMMO) solution (50 vol %), heated and stirred at 115 °C until it became transparent. 7.5 mL of dimethyl sulfoxide (DMSO) were added to the solution prior to spinning. The cellulose solution was spin-coated on the PVAm substrates at 5000 rpm for 40 s.

$EO_{19}PO_{29}EO_{19}$ Aqueous Solutions. $EO_{19}PO_{29}EO_{19}$ (BASF) is a triblock copolymer of ethylene oxide EO ($-C_2H_4O-$) and propylene oxide PO ($-C_3H_6O-$) terminating in primary hydroxyl groups (Figure 2). Its molecular weight and density at 20 °C are 3400 g/mol and 1.06 g/cm^3, respectively.

Triblock copolymers are known to form micelle structures in aqueous solutions.[25] The formation of micelles is induced with increased block copolymer concentration, above the critical micelle concentration (CMC) or exceeding the critical micellization temperature. The CMC of the $EO_{19}PO_{29}EO_{19}$ was determined via surface tension measurements (Du Nöuy method, Fisher Surface Tensionmat model 21, Fisher Scientific). The results indicate a critical micelle concentration of 0.0001%. This value is in good agreement with previous reported values.[26] All in situ AFM measurements reported here were performed at a 1% w/w concentration to guarantee that the solution was well above the CMC of $EO_{19}PO_{29}EO_{19}$.

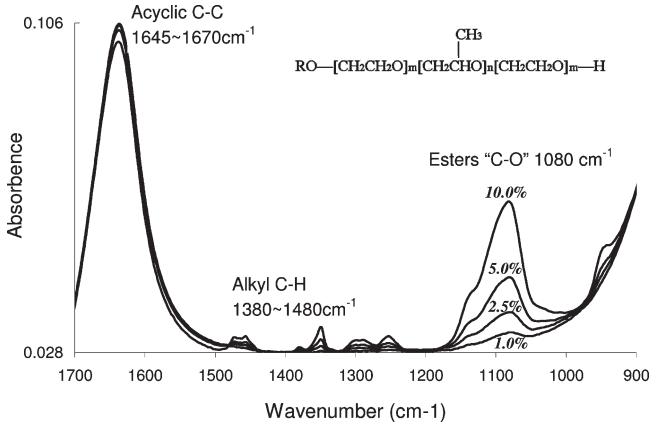

Figure 3. ATR-FTIR spectra of the $EO_{19}PO_{29}EO_{19}$ solutions (1.0, 2.5, 5, 10% by weight concentrations).

Table 1. Water Contact Angle for Silica, PP, PE, and Cellulose Surfaces

surface	contact angle (deg)
silica	26 ± 2
PP	103 ± 2
PE	95 ± 1
cellulose	29 ± 3

Chemical analysis of $EO_{19}PO_{29}EO_{19}$ solutions (at aqueous concentrations of 1%, 2.5%, 5%, and 10% by weight) was carried out via ATR-FTIR (Thermo Nicolet Magna-IR 560 Spectrometer) (see Figure 3) and three characteristic bands were analyzed: (1) the region of 1645−1670 cm^{-1}, assigned to the −OH band of both free and bound water in the system; (2) the region of 1380−1480 cm^{-1}, assigned to the hydrated state of $-CH_3$ and $-CH_2-$ surrounded by water, and (3) the band at 1080 cm^{-1}, assigned to the conjugation of the C−O−C stretching vibration of PPO and PEO blocks.[27] As expected, the intensity of these bands increased with solution concentration. This increase was especially prominent in the C−O−C bands, which play important roles in $EO_{19}PO_{29}EO_{19}$ chain mobility.

Water Contact Angle Measurements. Contact angles of Milli-Q water droplets on bare silica, PP, PE, and cellulose surfaces were measured by using a goniometer (Ramé-Hart, NJ). Ten microliters of Milli-Q water was placed onto the surface. Polymer coated specimens were immersed in an $EO_{19}PO_{29}EO_{19}$ solution (1% by weight) overnight, rinsed with Milli-Q water and dried with a dry nitrogen jet. The contact angles of the pristine surfaces are shown in Table 1.

According to Table 1, both PP and PE surfaces exhibit large contact angles (>90 degrees), while the cellulose surface has low contact angles (<90°). These values of contact angles indicated the hydrophobic/hydrophilic character of the substrate.

Molecular Dynamics (MD) Simulation. MD simulations of equivalent oligomeric species were carried out to quantify the affinity of the PEO and PPO chains of the triblock copolymer with the respective surface.[28]

Model Building. Simulations were performed using Materials Studio 4.1 from Accelrys Software Inc. (San Diego, CA). MD calculations were carried out using the Discover module[29] and COMPASS[30] (Condensed-phase Optimized Molecular Potentials for Atomistic Simulation Studies) force field. First, the (PP, PE, and cellulose) surfaces were

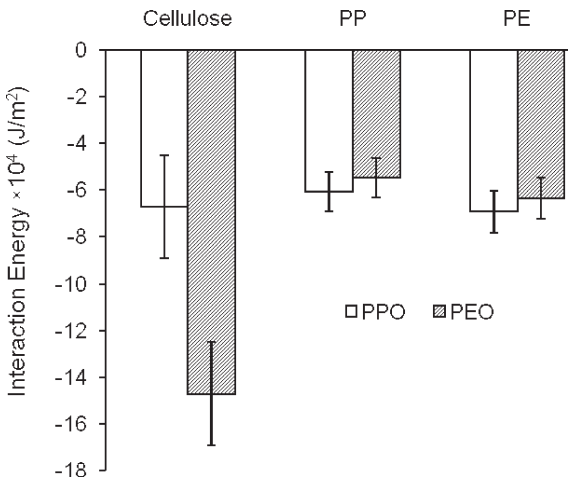

Figure 4. Simulated Interaction energy $E_{interaction}$ (J/m^2) of PPO and PEO blocks interacting with the cellulose, PP, and PE model surfaces.

constructed using the amorphous cell module developed by combining an algorithm by Theodorou and Suter[31] and the scanning method of Meirovitch.[32] The density of the PP, PE, and cellulose were chosen as 0.873, 0.848, and 1.446 g/cm^3, respectively.[33,34] The PP, PE, and cellulose oligomer chains were built by monomer units and then were placed into a 30 × 30 × 30 Å computational slab.

PEO and PPO slabs were created via the amorphous cell module using 24 PEO and 18 PPO oligomer chains in which each oligomer chain was composed of 15 EO or 15 PO monomers. The polymer slabs of EO or PO were piled up on the confined oligomeric surface of PP, PE, and cellulose. A 20 Å vacuum layer was placed above the polymer slab allowing the oligomers to expand freely in the z direction and preventing direct interaction between the atoms on the top and the bottom of the cell. MD simulations were performed under the constant volume and temperature (NVT) ensemble. Models built with 3D periodicity were equilibrated for 5 ps in the NVT ensemble at 298 K. Once equilibrated, the systems were subjected to 1000 ps of dynamics with the trajectories being saved every 1 ps during the last 100 frames to calculate the value of the interaction energy.

Interaction Energy. The interaction energy represents the amount of work necessary to separate a polymer block of EO or PO from the model surfaces. The interaction energy is hence proportional to the difference between the total energy of the system, E_{total}, and the energy of the individual layers, $E_{surface}$ and $E_{polymer}$. This energy difference should be normalizedin order to obtain the interaction energy at a molecular level. We adopted the surface area method reported by Chauve et al.[35] This method calculates the interaction energy of the polymer in the middle of a sandwich model by dividing the energy difference by twice the surface areas. Because there is only one interacting interface in our model, the energy difference is divided by the surface area of the computing cell, $S_{surface}$, hence obtaining the interaction energy, $E_{interaction}$ (J/m^2), as shown n eq 2.

$$E_{interaction} = -(E_{total} - E_{surface} - E_{polymer})/S_{surface} \quad (2)$$

The values calculated for the interaction energy are presented for the different polymer block-substrate pairs in Figure 4.

Surface Morphology of Adsorbed Polymers by Atomic Force Microscopy. An Atomic Force Microscope system (NTEGRA Prima, NT-MDT, Zelenograd, Russian Federation) was employed to characterize the topography of the bare and treated (with adsorbed triblock copolymer) substrates. Imaging of the substrates was performed in air (air-test), and under DI water (water-test). AFM imaging was also performed in 1% w/w aqueous solution of the triblock copolymer ($EO_{19}PO_{29}EO_{19}$-test). AFM scanning was performed in tapping mode using a MikroMasch (San Jose, CA) probe with a force constant of 0.35 N/m and resonance frequency of 145 Hz. During the water-test and EO_{19}-$PO_{29}EO_{19}$-test, the respective solutions were injected into a liquid metal cell coated with PTFE where the specimens were properly secured. All tests were performed with a scanning frequency of 1 Hz and a scan size of 500 nm and 1 μm. Topography and phase signals were collected and each image consisted of 256 × 256 pixels. Then, the images were analyzed using NOVA (an image analysis software of provided by NT-MDT) to produce two-dimensional Fast Fourier Transformation images and to calculate surface roughness, Ra.

RESULTS AND DISCUSSION

Model Surfaces. PP, PE, and cellulose thin films deposited on silica are shown in Figure 5a−c as AFM height images which were obtained in air. The PP surface imaged in air exhibits a fibrillar morphology (Figure 5a). Such structures may have formed after crystallization of PP during the spin-coating process.[36] In contrast to these fibrous-like structures, PE crystal structures appear as cones (Figure 5b) while the cellulose films displays rodlike crystal features.[37] In order to depict the molecular ordering or orientation in surface morphology, 2D Fast Fourier transform (2DFFT) images were derived for each corresponding surface of PP, PE, and cellulose and depicted in Figures 5d−f.

The surface morphology of PP and PE films appears to show more ordering or orientation at molecular level as shown in clear patterns in Figure 5a, b.[38] Instead, the 2DFFT image for cellulose substrate shows a more diffuse center. It is suggested that the cellulose surface was more amorphous and less ordered.[39] Line profiles are shown in Figure 5g−j as a means to determine the surface roughness (Ra). It was found that the PE surface exhibited the largest of Ra value (1.95 nm), whereas the smaller Ra calculated corresponded to cellulose, Ra = 0.565 nm. The Ra for the PP surface was determined to be 0.653 m.

Interaction Energy. Figure 6 shows the net $E_{interaction}$ calculated as the difference between individual block-surface interactions, i.e., $\Delta(E_{PPO\_surface} - E_{PEO\_surface})$. Positive values of $E_{interaction}$ indicate attractive pair potentials and negative values represent repulsive interactions. PEO blocks are shown to have a high affinity with the hydrophilic cellulose surfaces while the PPO blocks had a higher affinity with the PP and PE surfaces (Figure 6). In this latter case, the net interactions were higher for the more hydrophobic PP surface.[40] The differences in chemical affinities were expected to affect the self-assembling behavior of $EO_{19}PO_{29}EO_{19}$ molecules at the solid interface. For example, buoy−anchor−buoy structures of the PEO−PPO−PEO triblock copolymer can be predicted, as has been reported for similar polymers adsorbed on hydrophobized silica.[13,19,25] As can be derived from Figure 6, $EO_{19}PO_{29}EO_{19}$ molecules adsorbed on PP and PE surfaces with the PPO blocks acting as anchors while it is likely that the end PEO blocks were anchored on the hydrophilic cellulose. In all cases, the buoys segments are those with less affinity to the surface.

So far this discussion has addressed the case of adsorption of $EO_{19}PO_{29}EO_{19}$ as unimeric species, at submicellar concentrations. However, at concentrations above the CMC the associative behavior of the polymer has to be factored in, which makes the prediction of adsorbed architectures via MD simulation much more complex. Therefore, a better understanding of the

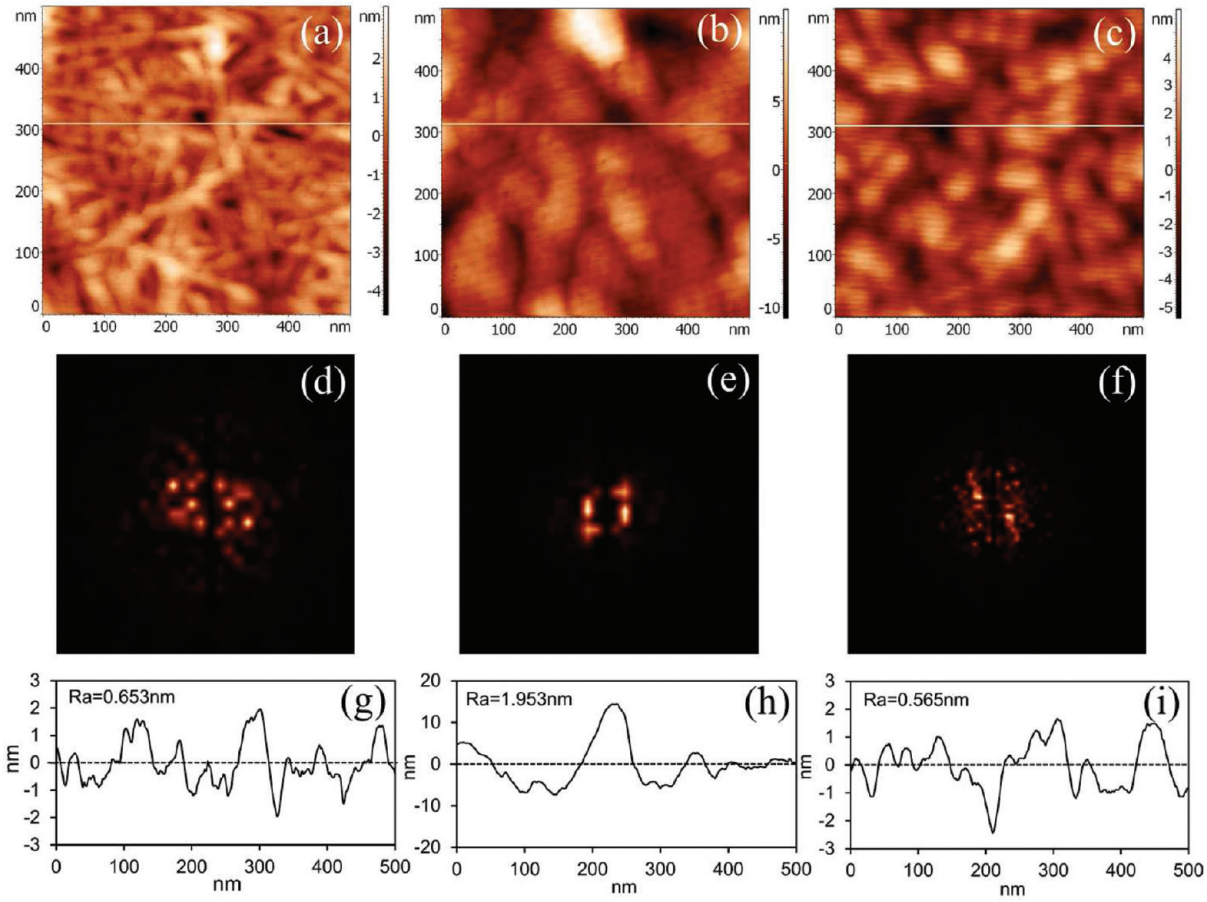

Figure 5. 500 nm AFM height images of spin-coated thin films of (a) PP, (b) PE, and (c) cellulose (images obtained in air). Respective 2D FFT images are provided for (d) PP, (e) PE, and (f) cellulose, as well as AFM line profiles: (g) PP, (h) PE, and (i) cellulose. Fibrillar morphologies are noted for PP surfaces, conical morphologies on the PE surface, and rodlike features re-observed on the cellulose surfaces. In addition, the PE surface shows higher surface roughness (Ra) than PP and cellulose surfaces, whereas the Ra of the PP surface is close to that of the cellulose surface.

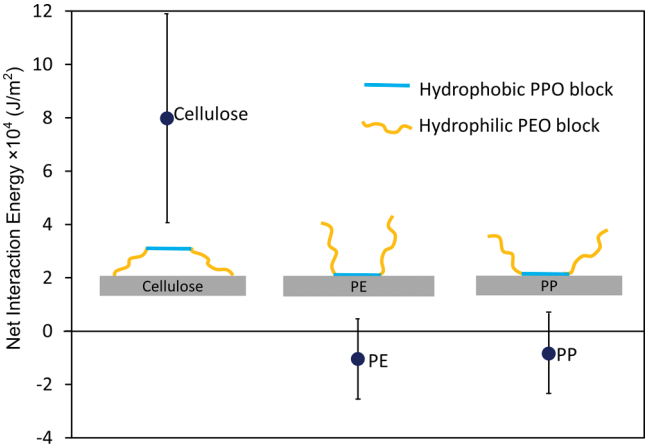

Figure 6. Net interaction energy, $\Delta(E_{PPO\_surface} - E_{PEO\_surface})$ of $EO_{19}PO_{29}EO_{19}$ adsorbing on cellulose, PE and PP surfaces. The relative larger affinity of PEO block with cellulose explains a net positive Δ(PPO_surface − PEO_surface). By contrast, the negative net interaction for PP and PE surfaces reveals larger affinity with the PPO block.

morphology of the adsorbed structures would be more challenging but more directly by experimental methods, such as AFM imaging, as discussed in the next section.

Adsorbed Structures. *Adsorption of $EO_{19}PO_{29}EO_{19}$ on PP.* AFM imaging in air (Figure 5a) revealed that $EO_{19}PO_{29}EO_{19}$ formed fibrillar structures after adsorption from aqueous solution above CMC on PP surfaces (see Figure 5a). Such features are observed more clearly when AFM imaging is conducted in water (in Figure 7a); this is mainly due to the improved lateral resolution as capillary forces between the tip and the surface vanish. The surface roughness, Ra, of the PP surface measured in water is 0.65 nm (Figure 7c), which is the same value measured in air, within the experimental error. When scanned in aqueous $EO_{19}PO_{29}EO_{19}$ solution, the crystallite, fiber-like structures are reduced or disappear, compared to the case when the surface is scanned in air (Figure 7b): in addition, a smaller surface roughness (Ra = 0.51 nm, see Figure 7d) was determined.

Molecular dynamic simulations indicate that $EO_{19}PO_{29}EO_{19}$ absorbs on hydrophobic PP surfaces with the PPO blocks anchored on the surface and PEO blocks dangling in solution, as buoys.[41] The anchoring of PPO blocks on the interface was initially probed by Kim et al., who studied molecular alignment of a PPO−PEO−PPO triblock copolymer at polystyrene/water interface using infrared-visible sum frequency generation (SFG) vibrational spectroscopy.[42] Therefore, it is believed that a buoy−anchor−buoy (B−A−B) structure was induced on the PP surface surrounding by the copolymer solution. It appears

~1nm, were observed.

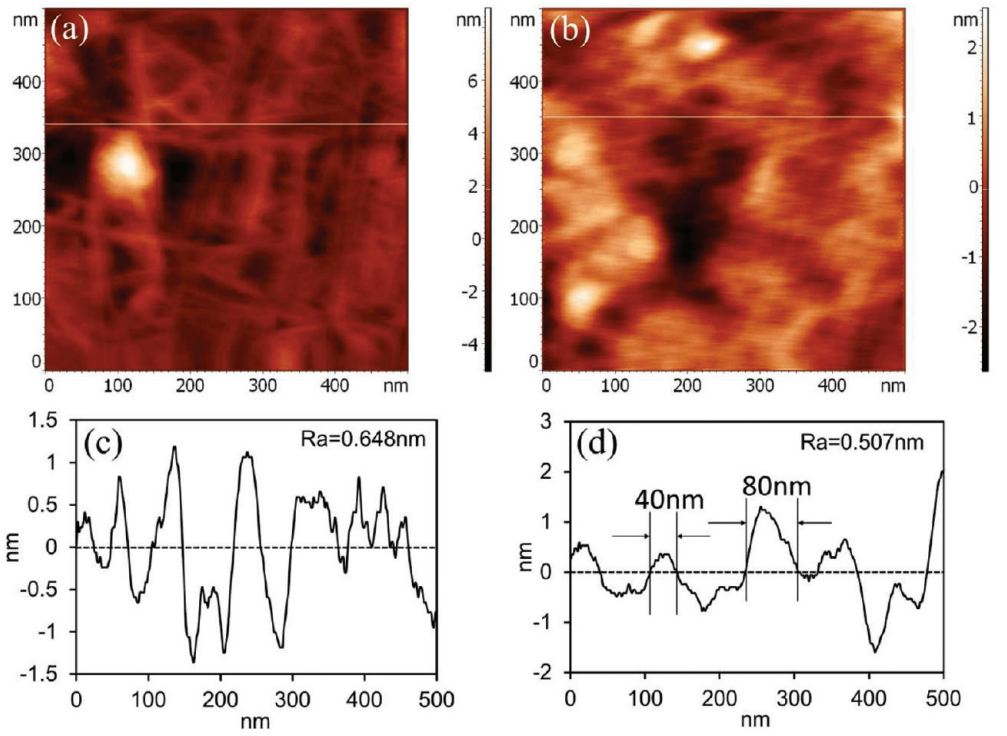

Figure 7. AFM height images of PP surfaces immersed in (a) water and (b) in $EO_{19}PO_{29}EO_{19}$ aqueous solution. Representative line profiles of the surface immersed in (c) water and (d) in $EO_{19}PO_{29}EO_{19}$ solution.

that the fibrillar structures observed in the case of bare PP were smoothed out by an adsorbed $EO_{19}PO_{29}EO_{19}$ layer, which is reflected by the reduction in surface roughness (Figure 7c and 7d). Furthermore, because the concentration of $EO_{19}PO_{29}EO_{19}$ used in AFM imaging, 1% w/w, was well above the critical micelle concentration (CMC of 0.0001% w/w) it is expected that micelles were present in solution. The line profile shown in Figure 7d indicates that the features detected by AFM had average sizes in the plane (horizontal) and out of plane (vertical) direction of 40−80 nm and 1−2 nm, respectively. Previous reports have indicated the formation of PEO−PPO−PEO triblock copolymer micelles in aqueous solution with an average radius of gyration of 8.6 nm and a diameter of 20−30 nm.[43] Therefore, the features observed under the AFM were larger but thinner. Unlike spherical configuration of common micelles, the ones we observed were two-dimensional aggregates. Earlier, Somasundaran et al. while studying sodium dodecyl sulfonate adsorption on alumina-water interface discovered similar two-dimensional aggregates, named hemimicelles, indicating that when the micelles in solution come into contact with a solid surface, they can be transformed from spherical micelles into hemimicelles.[44] Such transformation was induced by the affinity of PEO−PPO−PEO molecules to the surface. As the MD results indicated the strong interaction of PPO with the hydrophobic PP surfaces, The PPO blocks attach to the surface so as to create the buoy (PEO)−anchor (PPO)−buoy (PEO) structures. It is well-known that the PEO−PPO−PEO triblock copolymers form micelles in solution due to hydrophobic effect. However, at the interface, there are not only the hydration forces but also the interaction of the PEO−PPO−PEO molecules with the surface. For those micelles at the interface, the strong interaction of PPO with the hydrophobic PP surface also played a role so that these micelles were collapsed and deformed into hemimicelles on the surface. They become bigger and thinner on the surface. It is also worth noting that the height of these structures was in agreement with values reported by Liu et al. where the adsorption of $EO_{37}PO_{56}EO_{37}$ on silica surfaces was studied.[20] When the concentration of $EO_{37}PO_{56}EO_{37}$ was above CMC, globular aggregates with a vertical height of ∼1 nm, were observed.

Adsorption of $EO_{19}PO_{29}EO_{19}$ on PE. Circular "cone" structures were observed on bare PE surfaces, as shown in Figure 2e. During imaging of PE immersed in water, these cone domains become more circular (Figure 8a). The changes in the shape of these features are ascribed to the hydration of material when in contact with water. When PE was immersed in $EO_{19}PO_{29}EO_{19}$ solution, the small domains previously seen on the dry PE surface seem to merge forming larger ones. This behavior is similar to that observed on PP surfaces. The micelles which were located at the interface were likely deformed and transformed into hemimicelles. The B−A−B adsorbed $EO_{19}PO_{29}EO_{19}$ polymer structure was formed on the PE surface due to the relatively larger hydrophobicity of PE. The line profile shown in Figure 8d indicates the hemimicelles detected by AFM had average sizes in the plane (horizontal) and out of plane (vertical) direction of 190 nm and 1−2 nm, respectively. The $EO_{19}PO_{29}EO_{19}$ layer reduces the roughness of the bare PE surface, resulting in a much lower Ra (1.04 nm, Figure 8d).

Both PP and PE surfaces are covered with hemimicelles with the B−A−B structures attaching to the surfaces. However, a more detailed study on the differences between the adsorbed structures on these surfaces is deemed necessary by comparing surface roughness and the micelles' dimension in the presence of

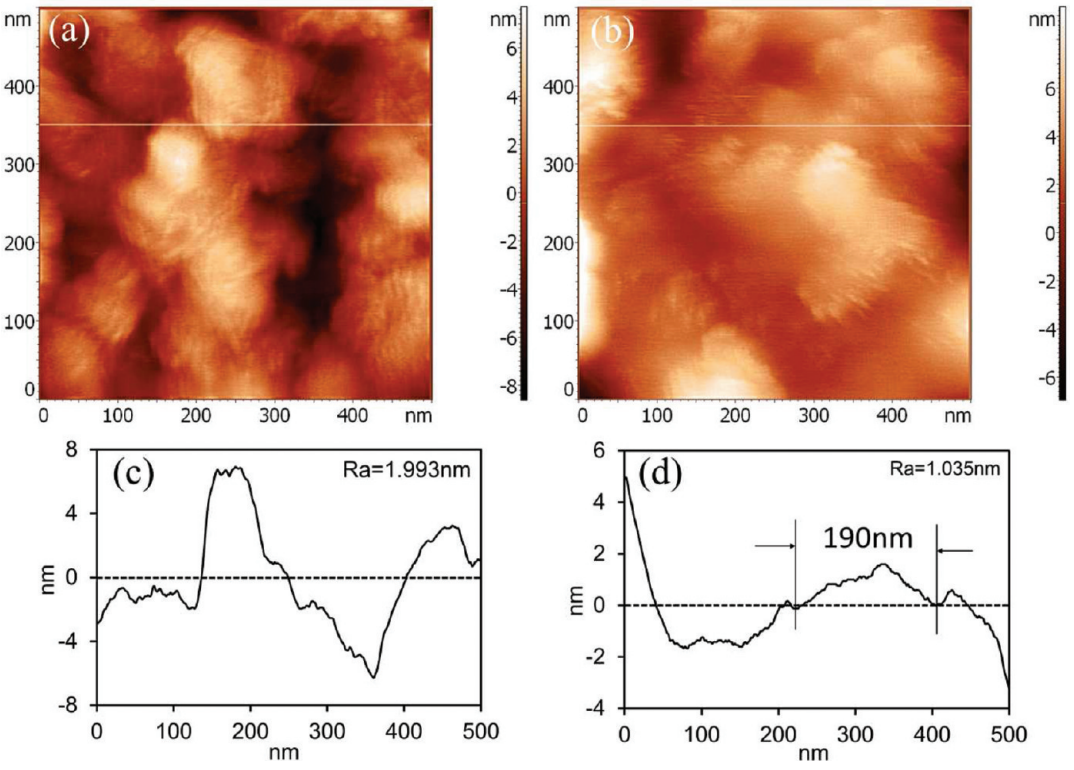

Figure 8. AFM height images of PE thin film in (a) water and in (b) $EO_{19}PO_{29}EO_{19}$ solution. Representive line profiles of the surface immersed (c) in water and (d) in $EO_{19}PO_{29}EO_{19}$ solution.

$EO_{19}PO_{29}EO_{19}$ solution. As a matter of fact, when obtained after scanning in $EO_{19}PO_{29}EO_{19}$ solution, the roughness for PE is reduced by 48% while that for PP is reduced by 22%. Another difference is that the in-plane dimension of the hemimicelles detected on PE surface, 190 nm, is even bigger than that on PP surface. The differences in surface roughness, in-plane dimension, can also be correlated with the self-assembled B−A−B structure. The affinity difference between the PPO and PEO block with the PE surface, $\Delta(E_{PPO\_PE}-E_{PEO\_PE})$, is actually slightly larger than that for the PP surface (see Figure 6). Therefore, compared with the PP surface, a larger stretching of the PEO blocks is expected when adsorbed on PE. The hemimicelles are even bigger due to the larger interaction of PPO with the PE surface. It is also due to the more stretched PEO chains on PE surfaces that the molecular ordering and packing in the hemimicelles is enhanced and the surface smoothness is increased, compared to the PP surfaces.

Adsorption of $EO_{19}PO_{29}EO_{19}$ on Cellulose. Reports on the adsorption of triblock copolymers on hydrophilic surfaces are less frequent than on hydrophobic ones.[45] AFM image of cellulose thin films, as shown in Figure 5c, indicated the presence of rodlike structures.[46] Figure 9a shows the morphology of the cellulose surface imaged while immersed in water. It is observed that the rodlike features disappeared and were substituted by globular ones. Therefore, it is possible that the changes in crystal configuration are mainly due its hydration. Figure 9b presents the morphology of the cellulose surface while immersed in the $EO_{19}PO_{29}EO_{19}$ solutions which are different than then ones observed in water. Compared with Ra = 0.590 in water, the surface roughness in $EO_{19}PO_{29}EO_{19}$ solution decreased and was 0.080. The line profile shown in Figure 9d indicates the features detected by AFM had average sizes in the plane (horizontal) and out of plane (vertical) direction of 30−80 and 0.3 nm, respectively.

The interaction energies obtained from MD simulations suggest that PEO has higher affinity with cellulose than the PPO block, Therefore, a different molecular configuration as that proposed on PE and PP, the reverse A-B-A model, is hereby proposed to form on the hydrophilic cellulose surface, as shown in Figure 6. A similar model was proposed previously by Wu et al. who used AFM to study the adsorption of an $EO_{99}PO_{69}EO_{99}$ triblock copolymer onto hydrophilic silica surfaces.[13] Unlike the hemimicelles on the PP and PE surfaces, the features on cellulose were still micelles with PPO blocks inside and PEO blocks outside. Because the bigger size in plane direction (30−80 nm) and smaller size out of plane direction (0.3 nm), compared with the reported micelles, they were flat micelles. In addition, the reverse A-B-A structure has a significant effect on the surface energy. The surface roughness of cellulose decreased by an 86% after exposure to $EO_{19}PO_{29}EO_{19}$ (Figure 9). It is thus possible that all buoy chains (PPO) in the $EO_{19}PO_{29}EO_{19}$ layer are parallel to the underlying surface. This structure is greatly beneficial to molecular ordering and packing of the layer. Therefore, the cellulose surface in the $EO_{19}PO_{29}EO_{19}$ solution is much smoother and well-ordered upon adsorption of $EO_{19}PO_{29}EO_{19}$.

In summary, when the three polymeric surfaces (PP, PE, and cellulose) were immersed in $EO_{19}PO_{29}EO_{19}$ solution, it is proposed that micellar structures are formed on the polymeric surfaces. It is hypothesized that hemimicelles formed on the PP and PE surfaces and flat micelles on cellulose surfaces, as illustrated in Figure 10. Because of the varied interaction between $EO_{19}PO_{29}EO_{19}$ molecules and surfaces, it is proposed that buoy−anchor−buoy structures form on PP and PE surfaces

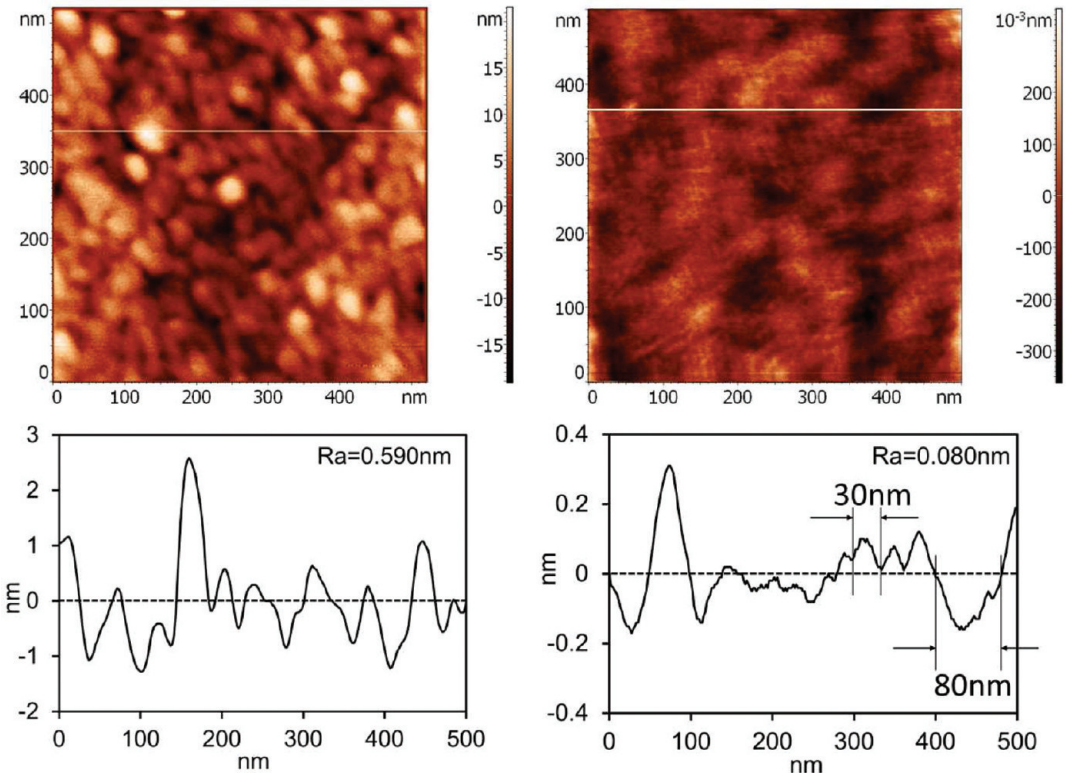

Figure 9. AFM height images of cellulose thin film (a) in water and (b) in $EO_{19}PO_{29}EO_{19}$ solution. Representative line profiles of the surface immersed (c) in water and (d) in $EO_{19}PO_{29}EO_{19}$ solution.

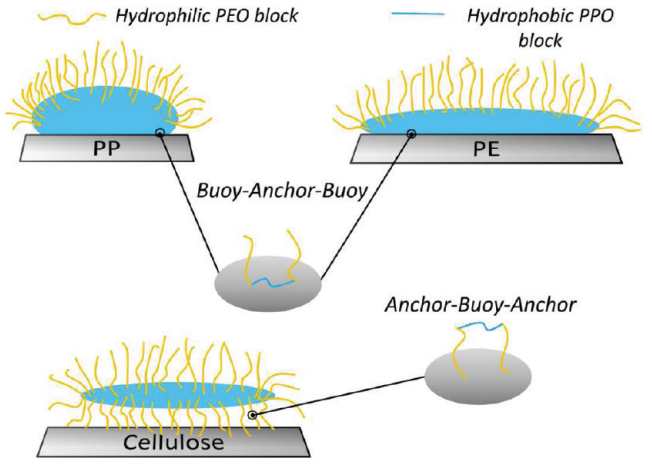

Figure 10. Scheme of proposed molecular configurations of $EO_{19}PO_{29}EO_{19}$ molecules induced on PP, PE, and cellulose surfaces. Hemimicelles are present on PP and PE surfaces and flat micelles on cellulose surface resembling a buoy−anchor−buoy BAB structure on PP and PE surfaces, and anchor−buoy−anchor ABA structure on the cellulose surface.

while anchor−buoy-anchor structures adsorbed cellulose surface. The amount of copolymer adsorbed on the solid surfaces was not addressed in this study. However, it has been reported by us and others that similar PPO−PEO−PPO copolymers adsorbed from aqueous solution onto solid surfaces in the range of 0.5−2 mg/m^2 and 0.1−0.2 mg/m^2 for hydrophobic and hydrophilic surfaces, respectively.[20,47,48]

CONCLUSIONS

Atomic force microscopy was employed to directly observe $EO_{19}PO_{29}EO_{19}$ self-assembly structures on PP, PE, and cellulose surfaces when the surfaces were immersed in solutions of $EO_{19}PO_{29}EO_{19}$ above the critical micelle concentration. AFM image analysis suggests that the micelles formed in the surface of the specimens were collapsed and transformed into so-called hemimicelles. Interaction energy calculations obtained via MD simulations illustrated that the PEO block have higher affinity with the cellulose surfaces than the PPO block, whereas the PPO has a higher affinity with PP and PE. The analysis of surface morphology and surface roughness suggests unique molecular configuration within the hemimicelles on the surface. The configurations of the triblock copolymer are found to be influenced by the nature of the substrate: a buoy (PEO)−anchor (PPO)−buoy (PEO) structure on the hydrophobic PP and PE is expected. On the other hand, an anchor (PEO)−buoy (PPO)−anchor (PEO) is proposed on the hydrophilic cellulose. Observation of these molecular assemblies via AFM may serve as a fundamental means to engineer better lubricant and additive systems for fiber processing operations.

AUTHOR INFORMATION

Corresponding Author

*Tel. +1-607 255 7600. Fax: +1-607 255 1093. E-mail: jh433@cornell.edu.

Present Addresses

$^{\nabla}$KAUST-Cornell Center for Energy and Sustainability, Cornell University, Ithaca, New York 14853, United States.

■ ACKNOWLEDGMENT

The authors acknowledge financial support by the National Textile Center under Grant Project C05-NS09.

■ REFERENCES

(1) Michielsen, S. J. *J. Eng. Fibers Fabr.* **2006**, *1*, 23–31.
(2) Behary, N.; Campagne, C.; Caze, C.; Perwuelz, A. *J. Appl. Polym. Sci.* **2003**, *89*, 645–654.
(3) Behary, N.; Caze, C.; Perwuelz, A.; El Achari, A. *Text. Res. J.* **2001** *71*, 187–194.
(4) Israelachvili, J. N. *Intermolecular and Surface Forces*; Academic Press: New York, 1992.
(5) Bhushan, B.; Israelachvili, J. N.; Landman, U. *Nature* **1995**, *374*, 607–616.
(6) Shubin, V. E.; Kékicheff, P. *J. Colloid Interface Sci.* **1993**, *155*, 108–123.
(7) Mate, C. M.; McClelland, G. M.; Erlandsson, R.; Chiang, S. *Phys. Rev. Lett.* **1987**, *59*, 1942–1945.
(8) Bhushan, B.; Liu, H.; Hsu, S. M. *J. Tribol.* **2004**, *126*, 583–590.
(9) Sasaki, N.; Kobayashi, K.; Tsukada, M. *Phys. Rev. B: Condens. Matter Mater. Phys.* **1996**, *54*, 2138–2149.
(10) Barrena, E.; Kopta, S.; Ogletree, D. F.; Charych, D. H.; Salmeron, M. *Phys. Rev. Lett.* **1999**, *82*, 2880–2883.
(11) Burns, A. R.; Houston, J. E.; Carpick, R. W.; Michalske, T. A. *Phys. Rev. Lett.* **1999**, *82*, 1181–1184.
(12) Zeng, H.; Maeda, N.; Chen, N.; Tirrell, M.; Israelachvili, J. *Macromolecules* **2006**, *39*, 2350–2363.
(13) Wu, C.; Liu, T.; White, H.; Chu, B. *Langmuir* **2000**, *16*, 656–661.
(14) Li, J.-T.; Caldwell, K. D.; Rapoport, N. *Langmuir* **1994**, *10*, 4475–4482.
(15) Schillen, K.; Claesson, P. M.; Malmsten, M.; Linse, P.; Booth, C. *J. Phys. Chem. B* **1997**, *101*, 4238–4252.
(16) Alexandridis, P.; Holzwarth, J. F.; Hatton, T. A. *Macromolecules* **1994**, *27*, 2414–2425.
(17) Malmsten, M.; Tiberg, F. *Langmuir* **1993**, *9*, 1098–1103.
(18) Fu, Z.; Santore, M. M. *Macromolecules* **1998**, *31*, 7014–7022.
(19) Brandani, P.; Stroeve, P. *Macromolecules* **2003**, *36*, 9492–9501.
(20) Liu, X.; Wu, D.; Turgman-Cohen, S.; Genzer, J.; Theyson, T. W.; Rojas, O. J. *Langmuir* **2010**, *26*, 9565–9574.
(21) Baranowski, R.; Whitmore, M. D. *J. Chem. Phys.* **1995**, *103*, 2343–2353.
(22) Wang, A.; Jiang, L.; Mao, G.; Liu, Y. *J. Colloid Interface Sci.* **2002**, *256*, 331–340.
(23) Marques, C.; Joanny, J. F.; Leibler, L. *Macromolecules* **1988**, *21*, 1051–1059.
(24) Song, J.; Liang, J.; Liu, X.; Krause, W. E.; Hinestroza, J. P.; Rojas, O. J. *Thin Solid Films* **2009**, *517*, 4348–4354.
(25) Patel, K.; Bahadur, P.; Guo, C.; Ma, J. H.; Liu, H. Z.; Yamashita, Y.; Khanal, A.; Nakashima, K. *Eur. Polym. J.* **2007**, *43*, 1699–1708.
(26) Diakova, B.; Kaisheva, M.; Platikanov, D. *Colloids Surf., A* **2001**, *190*, 61–70.
(27) Meng, S.; Sun, B.; Guo, Z.; Zhong, W.; Du, Q.; Wu, P. *Polymer* **2008**, *49*, 2738–2744.
(28) Prathab, B.; Subramanian, V.; Aminabhavi, A. T. M. *Polymer* **2007**, *48*, 409–416.
(29) Lippa, K. A.; Sander, L. C.; Mountain, R. D. *Anal. Chem.* **2005**, *77*, 7862–7871.
(30) Sun, H. *J. Phys. Chem. B* **1998**, *102*, 7338–7364.
(31) Theodorou, D. N.; Suter, U. W. *Macromolecules* **1985**, *18*, 1467–1478.
(32) Meirovitch, H. *J. Chem. Phys.* **1983**, *79*, 502–508.
(33) Derecskeia, B.; Derecskei-Kovacsa, A. *Mol. Simul.* **2006**, *32*, 109 115.
(34) Sun, C. *J. Pharm. Sci.* **2005**, *94*, 2132–2134.
(35) Chauve, G.; Heux, L.; Arouini, R.; Mazeau, K. *Biomacromolecules* **2005**, *6*, 2025–2031.
(36) Schönherr, H.; Wiyatno, W.; Pople, J.; Frank, C. W.; Fuller, G. G.; Gast, A. P.; Waymouth, R. M. *Macromolecules* **2002**, *35*, 2654–2666.
(37) Bartczak, Z.; Argon, A. S.; Cohen, R. E.; Kowalewski, T. *Polymer* **1999**, *40*, 2367–2380.
(38) Dissanayake, M.; Frech, R. *Macromolecules* **1995**, *28*, 5312–5319.
(39) Notley, S. M.; Wågberg, L. *Biomacromolecules* **2005**, *6*, 1586–1591.
(40) Wu, S. *Polymer Interface and Adhesion*; Marcel Dekker: New York, 1982.
(41) Eskilsson, K.; Tiberg, F. *Macromolecules* **1997**, *30*, 6323–6332.
(42) Kim, J.; Opdahl, A.; Chou, K. C.; Somorjai, G. A. *Langmuir* **2003**, *19*, 9551–9553.
(43) Alexandridis, P.; Hatton, T. A. *Colloids Surf., A* **1995**, *96*, 1–46.
(44) Somasundaran, P.; Fuerstenau, D. W. *J. Phys. Chem.* **1966**, *70*, 90–96.
(45) Eskilsson, K.; Tiberg, F. *Macromolecules* **1998**, *31*, 5075–5083.
(46) Lio, A.; Charych, D. H.; Salmeron, M. *J. Phys. Chem. B* **1997**, *101*, 3800–3805.
(47) Nelson, A.; Cosgrove, T. *Langmuir* **2005**, *21*, 9176–9182.
(48) Shar, J. A.; Obey, T. M.; Cosgrove, T. *Colloids Surf., A* **1999**, *150*, 15–23.